

# Homozygous ALS-linked *FUS* P525L mutations cell- autonomously perturb transcriptome profile and chemoreceptor signaling in human iPSC microglia

Sze Yen Kerk,<sup>1,\*</sup> Yu Bai,<sup>1</sup> Janell Smith,<sup>1</sup> Pranav Lalgudi,<sup>1</sup> Charleen Hunt,<sup>1</sup> Junko Kuno,<sup>1</sup> John Nuara,<sup>1</sup> Tao Yang,<sup>1</sup> Kathryn Lanza,<sup>1</sup> Newton Chan,<sup>1</sup> Angel Coppola,<sup>1</sup> Qian Tang,<sup>1</sup> Jennifer Espert,<sup>1</sup> Henderson Jones,<sup>1</sup> Casey Fannell,<sup>1</sup> Brian Zambrowicz,<sup>1</sup> and Eric Chiao<sup>1,\*</sup>

<sup>1</sup>Regeneron Pharmaceuticals, Tarrytown, NY 10591, USA

\*Correspondence: [eric.chiao@regeneron.com](mailto:eric.chiao@regeneron.com) (E.C.), [john.kerk@regeneron.com](mailto:john.kerk@regeneron.com) (S.Y.K.)

<https://doi.org/10.1016/j.stemcr.2022.01.004>

## SUMMARY

Amotrophic lateral sclerosis is a fatal disease pathologically typified by motor and cortical neurodegeneration as well as microgliosis. The *FUS* P525L mutation is highly penetrant and causes ALS cases with earlier disease onset and more aggressive progression. To date, how P525L mutations may affect microglia during ALS pathogenesis had not been explored. In this study, we engineered isogenic control and P525L mutant *FUS* in independent human iPSC lines and differentiated them into microglia-like cells. We report that the P525L mutation causes *FUS* protein to mislocalize from the nucleus to cytoplasm. Homozygous P525L mutations perturb the transcriptome profile in which many differentially expressed genes are associated with microglial functions. Specifically, the dysregulation of several chemoreceptor genes leads to altered chemoreceptor-activated calcium signaling. However, other microglial functions such as phagocytosis and cytokine release are not significantly affected. Our study underscores the cell-autonomous effects of the ALS-linked *FUS* P525L mutation in a human microglia model.

## INTRODUCTION

Amotrophic lateral sclerosis (ALS) is a fatal, progressive motor neurodegenerative disease for which no cure yet exists. A thorough understanding of its pathogenesis is hampered by the sporadic and idiopathic nature of the majority of disease instances. However, ~10% of ALS cases are familial and genetically linked. To date, mutations in >50 genes have been associated with familial and sporadic ALS, although the mechanisms by which they contribute to disease are poorly understood. Roughly two-thirds of familial occurrences can be attributed to mutations located in 4 genes: *C9ORF72*, *TARDBP*, *SOD1*, and *FUS* (Taylor et al., 2016). ALS-linked *FUS* mutations are highly penetrant and associated with earlier disease onset and more aggressive progression (Ji et al., 2017; Souza et al., 2015). The discovery that *FUS* protein mislocalization occurs in motor neurons of sporadic ALS patients also highlights its potential role in the majority of ALS cases (Tyzack et al., 2019). Despite extensive research, the exact cell types underlying ALS etiology are still unclear even for disease instances driven by familial mutations (Hickman et al., 2018).

*FUS* is a ubiquitously expressed gene. In the human adult central nervous system (CNS), it seems to be more highly transcribed in microglia compared to neurons and other glial cells (Zhang et al., 2016). The *FUS* protein is predominantly nuclear due to its nuclear localization signal (NLS) and can undergo liquid-liquid phase separation owing to its prion-like domains (Portz et al., 2021). *FUS* also possesses RNA- and DNA-binding domains and has

been functionally implicated in DNA repair and RNA processing such as transcription, splicing, transport, and translation. More than 50 mutations in *FUS* have been identified in families afflicted with ALS. The majority are dominant missense mutations largely clustered within the NLS or prion-like domains of the protein. One such mutation found in the NLS, P525L, causes juvenile-onset forms of ALS that are highly aggressive and penetrant (Kuang et al., 2017; Shang and Huang, 2016).

Pathologically, ALS is typified not just by motor and cortical neurodegeneration but also by microgliosis, where microglia become activated, change their morphology, gene expression, and exhibit altered motility, phagocytosis, and cytokine release functions (Clarke and Patani, 2020; Li and Barres, 2018). To date, how *FUS* P525L mutations may affect microglia during ALS pathogenesis had not been explored. To bridge this knowledge gap, we postulated that microglia derived from human induced pluripotent stem cells (iPSC) harboring *FUS* P525L would display transcriptional and functional changes. To test this hypothesis, we generated isogenic control and P525L mutant *FUS* using CRISPR (clustered regularly interspaced short palindromic repeats) technology in 2 independent human iPSC lines. The engineered cell lines possessing the series of *FUS* genotypes were then differentiated into microglia-like cells (MIGs). Immunocytochemistry demonstrated that the P525L mutation caused *FUS* protein to be mislocalized from the nucleus to the cytoplasm. RNA sequencing (RNA-seq) and intracellular calcium flux assays revealed that homozygous *FUS* P525L mutations perturbed the transcriptome profile and specific chemoreceptor signaling of





MIGs. However, other microglial functions such as phagocytosis and cytokine release were not significantly altered when examined by a panel of *in vitro* assays. Our study underscores the cell-autonomous effects of the ALS-linked *FUS* P525L mutation in a human microglia model.

## RESULTS

### CRISPR engineering of *FUS* P525L mutations and isogenic controls in independent human iPSC lines

Considering its penetrant and aggressive pathogenicity in ALS, we focused on the *FUS* P525L point mutation (Nauermann et al., 2019), located in the NLS region (Figure 1A), to study its effects on human iPSC-derived MIGs. Due to our lack of access to P525L patient samples, we engineered a *FUS* genotypic series of P525L mutations in 2 independent wild-type (WT) human iPSC lines, AG (Figure 1B) and JK (Figure S1A), to minimize any line-specific phenotypic differences due to their unique genetic backgrounds. The parental WT iPSC lines were derived by reprogramming 2 independent fibroblast lines using non-genome-integrating factors. Via CRISPR technology, *FUS* P525L homozygotes (Hom) were generated from WT iPSC lines using a single guide RNA (sgRNA), in which the middle nucleotide of the protospacer-adjacent motif (PAM) shared the same position as the desired point mutation. This obviated the need to introduce silent mutations within the single-stranded oligodeoxynucleotide (ssODN) repair template to prevent Cas9 re-cutting upon successful targeting. To generate P525L heterozygotes (Het), equimolar amounts of the mutant ssODN and a control ssODN containing 2 synonymous point mutations to prevent Cas9 re-cutting were used. By using this strategy, engineered controls (eCtrl) that were repaired biallelically with control ssODN were also obtained and treated as putative WT equivalents. Quality controls were performed via array comparative genomic hybridization (aCGH) to ensure no gross karyotypic abnormalities and single-nucleotide polymorphism (SNP) microarrays to exclude clones with copy-neutral loss-of-heterozygosity (CN-LOH) affecting entire chromosome arms (Figure S1C) (Weisheit et al., 2020). In summary, 2 independent, karyotypically normal, isogenic iPSC series of *FUS* genotypes encompassing WT, eCtrl, P525L Het, and P525L Hom were successfully engineered.

We also generated a *FUS* knockout (KO) clone in the iPSC AG line by biallelically deleting the entire *FUS* coding sequence using flanking sgRNAs (Figure 1B). Immunocytochemistry with an antibody against the *FUS* protein showed largely nuclear signals in both WT and eCtrl clones as expected and no detectable signal in the KO, confirming the successful deletion of *FUS* as well as the specificity of the anti-*FUS* antibody. Of particular note is the characteristic

*FUS* exclusion from nucleolar regions in the nucleus as previously reported (Yang et al., 2015). In P525L Hom, *FUS* was predominantly seen in the cytoplasm due to both chromosomal copies having mutated NLS, whereas in P525L Het cells, *FUS* was observed in both the nucleus and cytoplasm, likely representing the WT and mutant forms, respectively (Figures 1C and S1B). These observations of *FUS* subcellular localizations further confirmed the various genotypes of engineered iPSC lines and are consistent with published *FUS* immunostaining results in human fibroblasts from P525L mutation carriers (Lo Bello et al., 2017).

### Directed differentiation of human iPSC lines with *FUS* P525L mutations and isogenic controls into MIGs

To study the effects of *FUS* P525L mutation in human microglia, we adopted the established protocol from Douvaras et al. (2017) to sequentially direct the differentiation of our CRISPR-engineered iPSC lines through an initial mesodermal lineage, followed by an intermediate myeloid progenitor stage, and finally into MIGs (Figure 2A). This strategy attempted to recapitulate the differentiation process of microglia during embryonic development, which was elucidated a decade prior (Ginhoux et al., 2013). In our pilot experiment, iPSC AG lines with the following genotypes were differentiated: *FUS* WT, eCtrl, P525L Het (2 clones), P525L Hom (2 clones), and KO. The experimental design encompassed 4 differentiation replicates per iPSC clone and myeloid progenitor harvests at 4 different time points. At the intermediate stage, adherent precursor cells continually generated free-floating myeloid progenitors marked by the membrane protein CD14 (Figures S2A and S2B), which were then periodically harvested, plated, and further differentiated into MIGs by applying interleukin (IL)-34, the CSF1R ligand in the brain that is crucial for microglia development (Wang et al., 2012). This pilot aimed to validate the molecular identity of the differentiated MIGs and determine its reproducibility across different harvest time points.

Immunosurveillance is one of the characteristic functions of microglia whose ramified processes continuously surveil the extracellular microenvironment for foreign or unwanted matter, which is then internalized via phagocytosis (Prinz et al., 2019). The iPSC lines of the *FUS* genotypic series gave rise to MIGs with motile pseudopodia and putative phagosomes migrating from cell edge to soma (Figure 2B; Videos S1A and S1B). These cells expressed microglial markers such as P2RY12, CX3CR1, MERTK, MRC1, and TREM2 at percentages that were well within reported ranges (Figures 2C and 2D) (Douvaras et al., 2017). Many of these marker proteins have well-established microglial functions such as target recognition, chemotaxis, and apoptosis (Prinz et al., 2019). Also confirmed was the expression of MEF2C, a transcription factor hypothesized

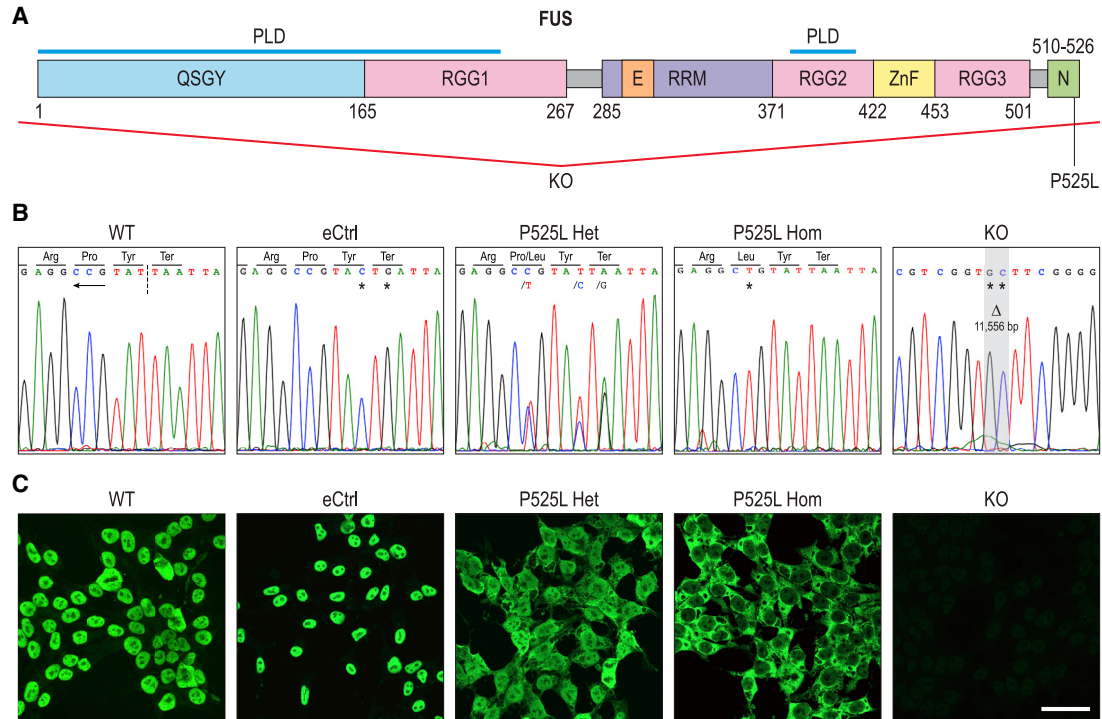


**Figure 1. CRISPR engineering of *FUS* P525L mutations and isogenic controls in independent human iPSC lines**

(A) Schematic of human *FUS* protein and its domains. QSGY and RGG, regions rich in the stated amino acids; PLD, prion-like domain; E, nuclear export signal; RRM, RNA recognition motif; ZnF, zinc finger domain; N, NLS. Numbers indicate amino acid positions. Red lines denote deletion of the entire *FUS* coding sequence in the KO.

(B) Sanger sequencing of CRISPR-engineered *FUS* genomic locus in human iPSC lines. In the WT panel, the inverted NGG PAM site is underlined by the arrow, whereas the Cas9 endonuclease cut site is bisected by the perforated line. Homozygous point mutations compared to WT, such as that in P525L Hom, are denoted by asterisks. Heterozygous point mutations such as those in P525L Het are denoted by a slash, followed by the mutant allele. In the KO, the gray area represents a homozygous deletion ( $\Delta$ ) of 11,556 bp containing the entire *FUS* coding sequence, substituted by 2 point mutations.

(C) Immunocytochemistry of *FUS* protein revealing its subcellular localization in iPSCs of different genotypes. To better visualize the cytoplasmic compartment, iPSCs were dissociated into single cells and plated with ROCK inhibitor Y-27632, which causes cells to stretch out on the culture surface. Apparent variations in cell size are due to fixations being performed at different stages of cell-plate adherence. Scale bar, 50  $\mu$ m. Presented here are clones from the AG line; see Figure S1 for the JK line.

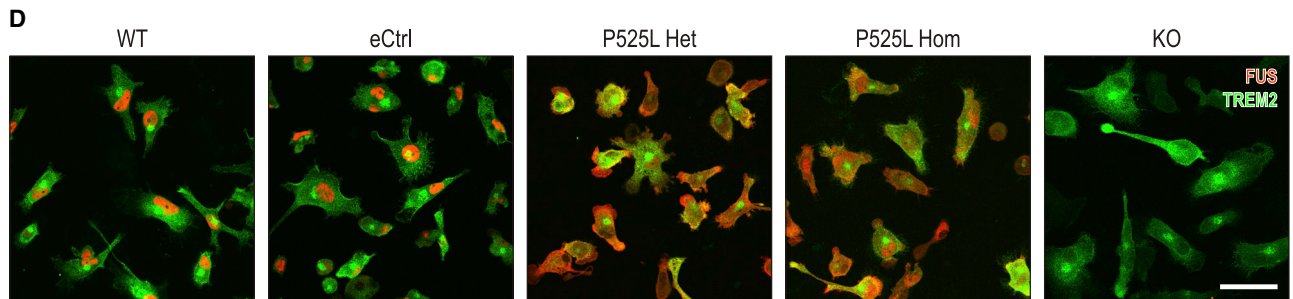
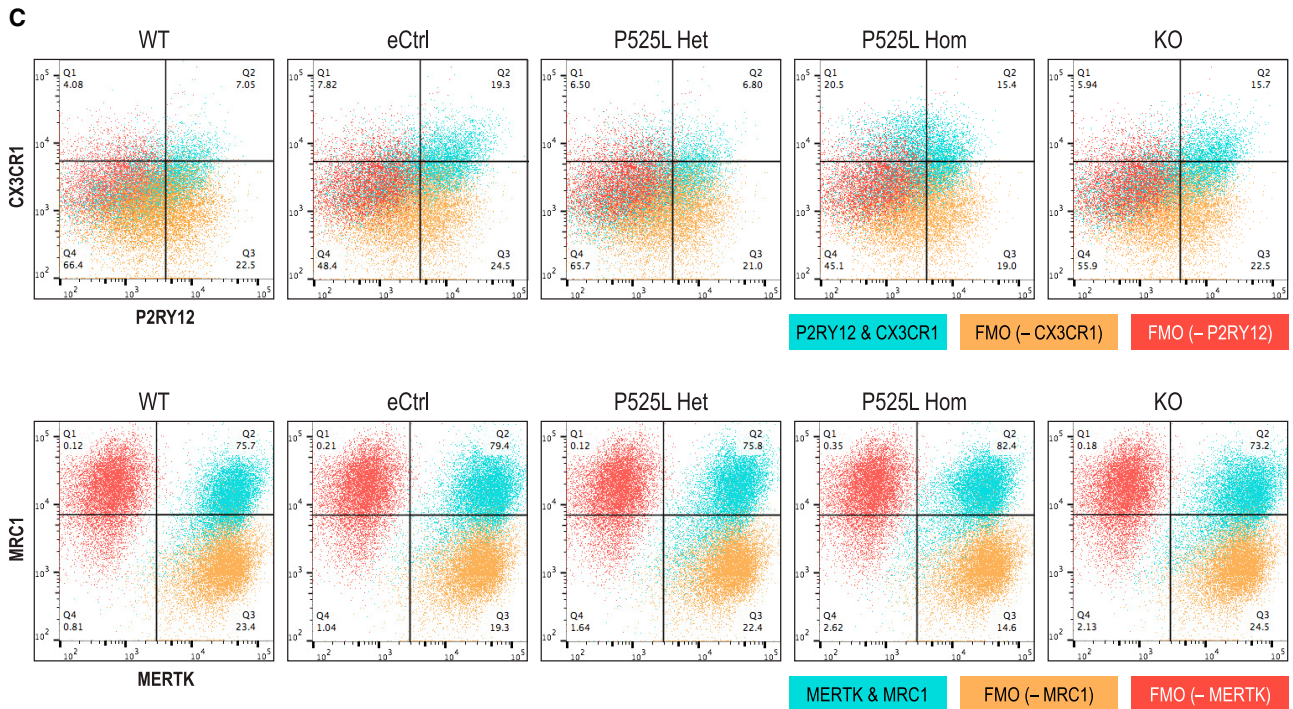
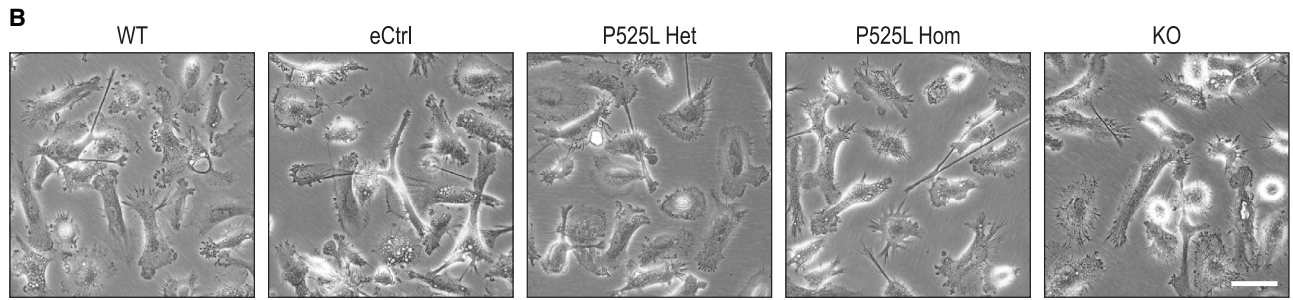
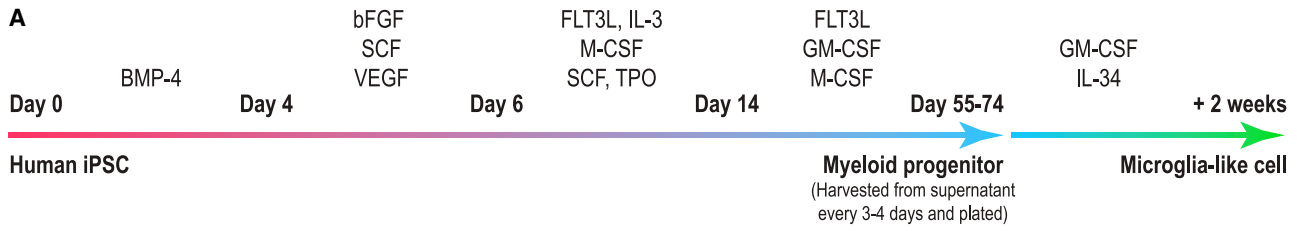
to specify microglial identity (Lavin et al., 2014), as well as TBK1 and MAP3K7 (Figure S2C). A heterozygous *Tbk1* mouse model with *Map3k7* heterozygosity spatially induced in myeloid cells displayed ALS-like neurodegeneration phenotypes (Xu et al., 2018). In addition, *FUS* subcellular localizations in MIGs across the different genotypes mirrored those observed in corresponding iPSCs as expected (Figures 1C and 2D).

#### Identity validation via RNA-seq of iPSC-derived MIGs with *FUS* P525L mutations and isogenic controls

In the pilot transcriptome profiling experiment, the MIGs of the *FUS* genotypic series and their preceding myeloid progenitors were subjected to next-generation RNA-seq. Principal component analysis (PCA) of transcriptome profiles showed that MIGs were differentiated from their progeni-

tors as these 2 groups clustered distinctly from each other (Figures 3A and 3B). This analysis also revealed that cells of different *FUS* genotypes were very similar in transcriptome profiles and grouped closely together, although P525L Hom cells clustered slightly away from the other genotypes, hinting at significant transcriptional perturbations due to the homozygous mutation (Figure 3A). Moreover, PCA demonstrated that MIGs terminally differentiated from progenitor cells harvested from the first 3 time points between days 52 and 75 of differentiation were quite similar and clustered closely together, in contrast to those from day 115 (Figure 3B). As such, in subsequent differentiation and RNA-seq experiments, we would harvest cells from the earlier time points to be used as replicates.

We next compared the transcriptome profiles of our MIGs to those of purified human cortical microglia and



(legend on next page)



brain cortex as published by Galatro et al. (2017). The authors extracted RNA directly from isolated cells without an intervening *in vitro* culture step, which has been shown to alter the microglial transcriptome profile within 6 h (Gosselin et al., 2017). Qualitatively, the global gene expression patterns of the MIGs of various *FUS* genotypes were more similar to those of purified primary human microglia as opposed to brain cortex (Figure 3C). Quantitatively, this was corroborated by the higher Spearman's rank correlation coefficients calculated between the gene expression profiles of MIGs with primary microglia ( $0.7766 \pm 0.0100$ ) compared to those between MIGs with brain cortex ( $0.4799 \pm 0.0050$ ). The latter values were much closer to the coefficient calculated between primary microglia and cortex (0.4620) (Figure 3D). That the global gene expression pattern of our microglia-like cells was not identical to that of primary microglia indicates that there is room for optimization of this differentiation protocol; our results should thus be viewed with this caveat in mind.

At the individual gene level of our MIGs, we confirmed the expression of multiple microglial markers (Figures 3E and S3A), which have been well defined (Butovsky et al., 2014; Hickman et al., 2013) and widely referenced by other researchers to validate the identity of their iPSC-derived microglia (Abud et al., 2017; Douvaras et al., 2017; Muffat et al., 2016; Pandya et al., 2017). The mRNA levels of these genes were consistent across genotypes and the first 3 time points, while a lower trend was seen in cells from day 115, supporting our decision to exclude later time points from subsequent experiments (Figures 3E and S3A). It is worthy of note that the expression level of the microglial marker *TMEM119* was extremely low in our MIGs (Figure S3A) (Bennett et al., 2016), as was also observed by Abud et al. (2017) and Douvaras et al. (2017). The immunocytochemistry and transcriptome profiling results from our pilot experiment demonstrated the consistent generation of iPSC-derived MIGs across different *FUS* genotypes between days 52 and 75, whereas cells harvested beyond day 100 seemed to exhibit a downregulation of microglial markers.

### Homozygous *FUS* P525L MIGs display transcriptional perturbations of genes associated with characteristic microglial functions

With the insights gained from our pilot studies, we proceeded to perform a larger-scale microglial differentiation

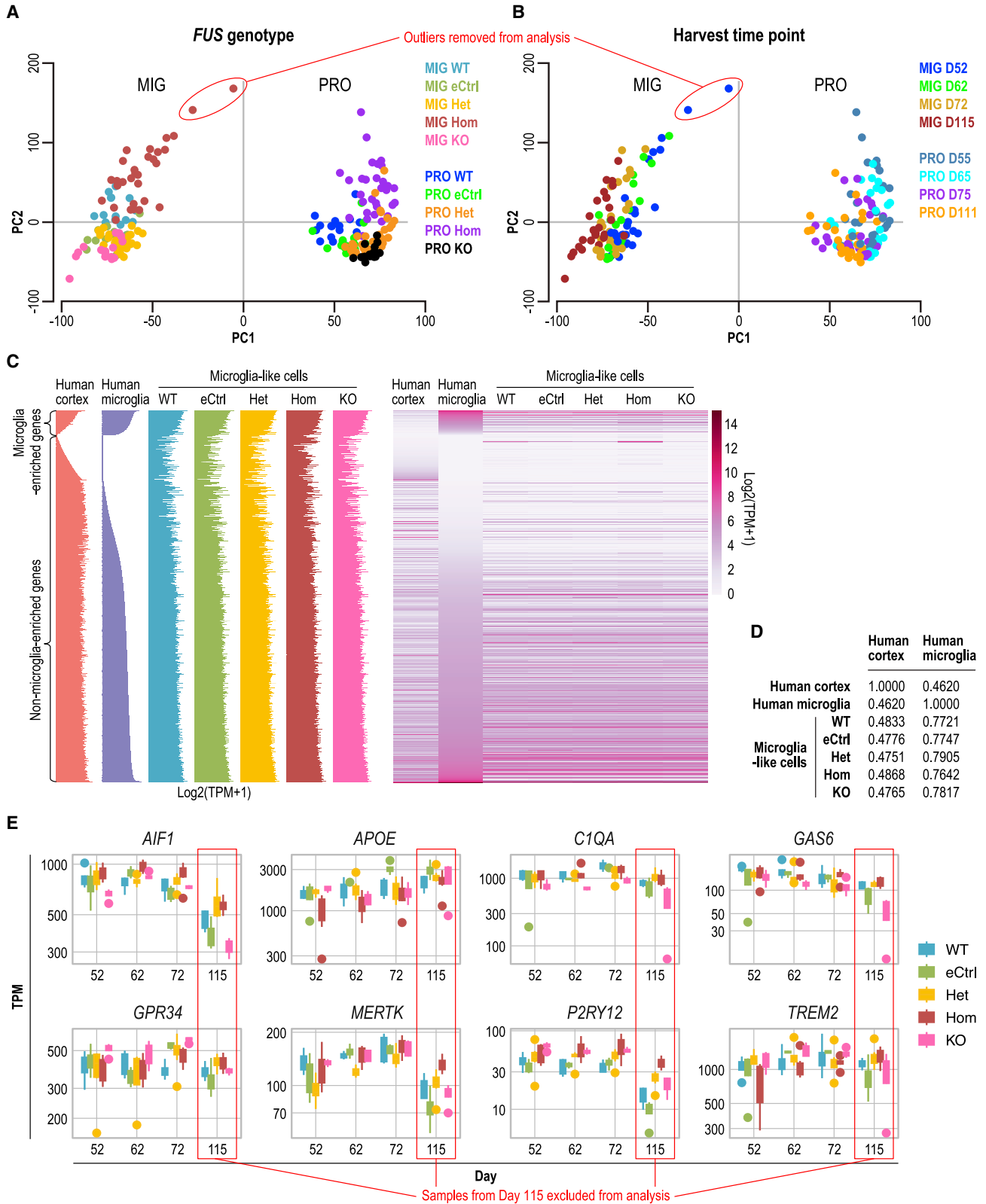
experiment with both independent human iPSC lines, AG and JK, harboring the series of *FUS* WT, eCtrl, P525L Het, and P525L Hom genotypes. The experimental design encompassed 2 independent differentiation experiments whereby for each differentiation run, myeloid progenitors were harvested at 4 different time points between days 55 and 74 and terminally differentiated into MIGs as described above (Figure 4A). Following RNA-seq, PCA of the transcriptome profiles showed that MIGs across genotypes, replicates, and time points clustered together and were similar in identity (Figure 4B). A minor issue with the clonality of the JK WT line uncovered via RNA-seq is addressed in Figure S4B. In short, this line was contaminated with a small percentage of cells containing undesired CRISPR mutations in the *FUS* locus that fortuitously did not alter the *FUS* WT amino acid sequence. As such, data from this line were included in our analysis.

A closer look at *FUS* gene expression revealed that it was significantly increased in P525L Hom compared to WT and eCtrl; in P525L Het, the expression level was intermediate between that of Hom and controls (Figure 4C). Such an observation was expected since *FUS* binds to a highly conserved region around exon 7 and flanking introns of its own pre-mRNA and partially represses exon 7 splicing. This repression causes exon 7 skipping in a portion of transcripts where resultant variants undergo nonsense-mediated decay, which decreases overall *FUS* transcript levels. The ALS-causing mutations in *FUS* NLS, R521G and R522G, have been documented to disrupt this negative autoregulatory function, hence explaining the upregulation of *FUS* gene expression in MIGs with the P525L allele (Zhou et al., 2013).

To address the question of whether the *FUS* P525L mutation causes any transcriptional perturbations in human microglia, we compared the transcriptome profiles of MIGs of Het and Hom genotypes with those of WT and eCtrl. Differential gene expression levels were defined as significantly different by a transcript fold-change threshold of no less than 1.5 in either the up or down direction as well as a *p* value cutoff of <0.01. Comparisons were always performed individually in each independent line, AG and JK, before filtering for the overlap of the results. *FUS* eCtrl MIGs were compared to WT and only 6 differentially expressed genes were observed (Table S1), validating our assumption that eCtrl is indeed equivalent to WT. Next, strict analysis criteria were used whereby gene expression levels in a

## Figure 2. Directed differentiation of human iPSC lines with *FUS* P525L mutations and isogenic controls into MIGs

- Schematic of differentiation protocol of human iPSCs into MIGs.
- Phase-contrast images of iPSC-derived MIGs of different *FUS* genotypes. For time-lapse movies depicting motile pseudopodia and putative phagosomes, see Videos S1A and S1B.
- Flow cytometry dot plots of characteristic microglial surface markers in MIGs. FMO, fluorescence minus 1 control using WT cells.
- Immunocytochemistry of *FUS* and microglial protein TREM2 in MIGs. Scale bar, 50  $\mu\text{m}$ . Presented here are clones from the AG line.



(legend on next page)



mutant genotype were compared to those in WT or eCtrl independently, and only genes that were differentially expressed in the same direction against both controls were considered to be a mutant signature. Through this analysis, only 1 Het signature gene emerged (Table S1), which led us to postulate that the effects of P525L Het, if any, could be too weak for detection in this system.

Homozygous *FUS* P525L mutation may yield stronger and more experimentally robust phenotypes compared to heterozygotes due to dosage effects. By applying the same strict criteria, we detected a total of 120 differentially expressed genes in the MIG P525L Hom signature, whereby 90 were upregulated and 30 were downregulated (Figure 4D; Table S1). Gene Ontology (GO) enrichment analysis revealed that the Hom signature is enriched for genes associated with GO terms linked to inflammatory response, cell motility, chemotaxis, leukocyte migration, antigen processing and presentation, and cytokine production, which are characteristic features and functions of microglia (Figure 4E). However, analysis using the Molecular Signatures Database (MSigDB) with a focus on Canonical Pathways yielded “G protein-coupled receptor (GPCR) ligand binding” as the second top term with Hom signature gene enrichment (Figure S4A). Several of these GO and MSigDB categories share the same constituent genes (Table S2) and the differential expression levels of 20 of these genes were orthogonally validated using quantitative reverse transcriptase-PCR (qRT-PCR), the qualitative results of which corroborated those obtained via RNA-seq (Figure 4F; Table S3).

### Differentially expressed chemoreceptor genes in MIGs with *FUS* P525L mutations lead to perturbations of ligand-induced intracellular calcium signaling

*P2RY6*, *GPR183*, *S1PR1*, and *CCR6* stood out as *FUS* P525L Hom signature genes encoding relatively well-studied G protein-coupled chemoreceptors with known biological ligands. The activation of *P2RY6* by uridine diphosphate (UDP) nucleotides (Koizumi et al., 2007), *GPR183* by  $7\alpha,25$ -dihydroxycholesterol (OHC) hydroxycholesterols

(Preuss et al., 2014), sphingosine-1-phosphate receptor 1 (*S1PR1*) by S1P (Lee et al., 2017), and *CCR6* by *CCL20* (Liao et al., 2002) converge downstream on intracellular calcium flux, a common signal transduction pathway of GPCRs. To investigate whether the increased expression of these chemoreceptor genes in *FUS* P525L Hom MIGs translates into a functional phenotypic difference compared to WT and eCtrl, intracellular calcium flux assays were performed using the ligand of each receptor. We noted that our MIGs responded to UDP and  $7\alpha,25$ -OHC (Figures 5A and 5B), but no response to S1P and *CCL20* was detected, even at high concentrations (Figures S5B and S5C).

Focusing on UDP and  $7\alpha,25$ -OHC, we proceeded to treat our MIGs of all 4 genotypes with these 2 ligands. Relative to WT and eCtrl, whose responses were not significantly different between the 2 as expected, intracellular calcium flux was significantly higher in P525L Hom when treated with UDP and  $7\alpha,25$ -OHC, respectively (Figures 5C and 5D). Despite not having a discernible differential gene expression signature, P525L Het cells also seemed to respond to UDP or  $7\alpha,25$ -OHC in terms of calcium flux compared to WT and eCtrl, albeit with a lower magnitude and less reliably compared to Hom. Calcium signals were greatly diminished when MRS2578 and NIBR189, potent specific inhibitors of *P2RY6* and *GPR183*, respectively, were applied to the cells before ligand addition (Figures 5C and 5D). These findings were consistently reproduced in P525L Hom MIGs derived from both independent iPSC lines and across both independent differentiations. These observations signify that transcriptional perturbations due to *FUS* P525L mutant alleles in MIGs, causing *P2RY6* and *GPR183* gene expression upregulation, led to the disruption of intracellular calcium signaling downstream from the ligand activation of these chemoreceptors.

### MIGs with *FUS* P525L mutations do not exhibit phagocytosis or cytokine release phenotypes

As opposed to their encounter with foreign pathogens, which triggers a large immune response, macrophages

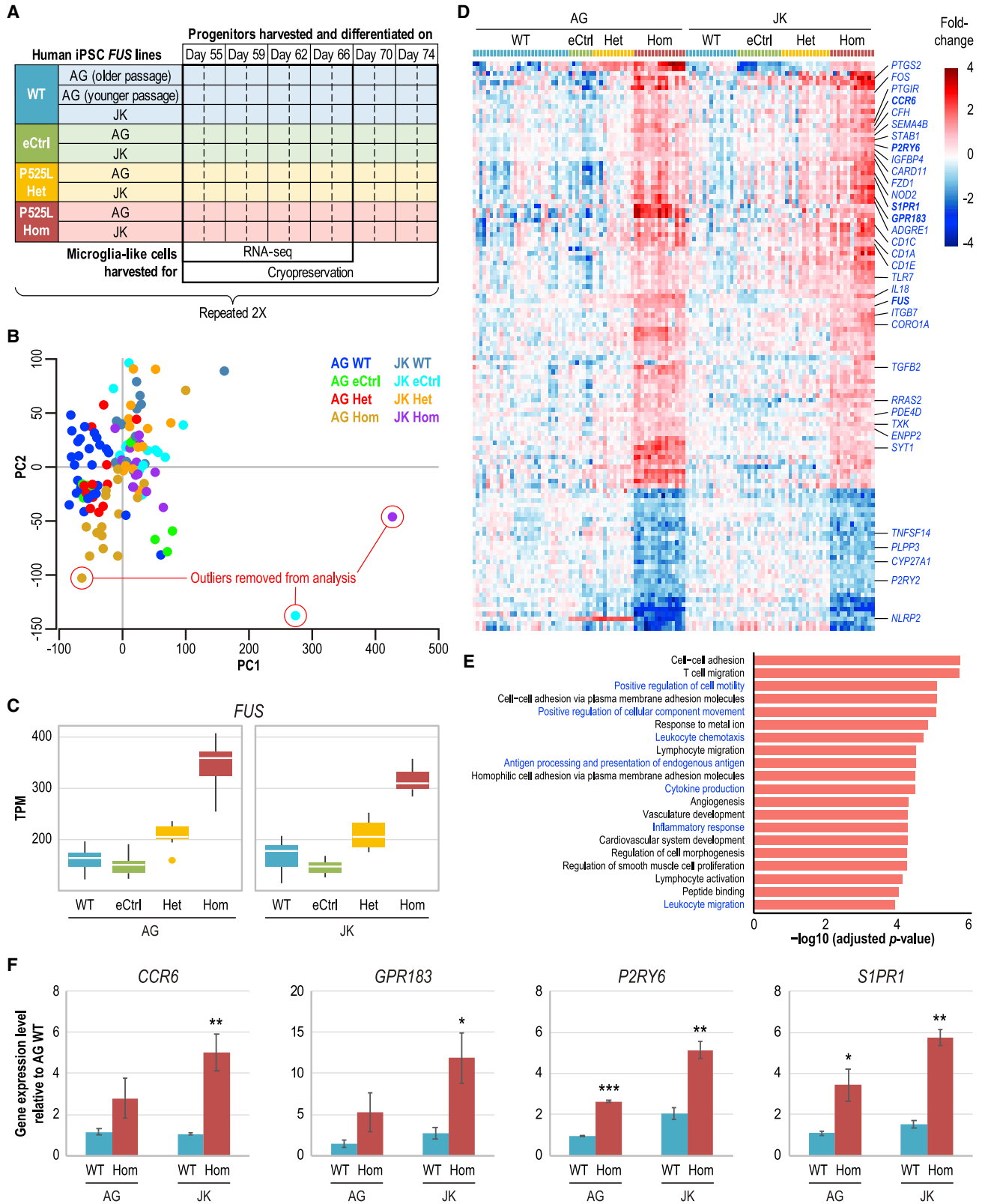
## Figure 3. Identity validation via RNA sequencing (RNA-seq) of iPSC-derived MIGs with *FUS* P525L mutations and isogenic controls.

(A and B) PCA of transcriptome profiles from RNA-seq of MIGs and their preceding myeloid progenitors (PRO). Color code indicates the different (A) *FUS* controls and P525L mutant genotypes or (B) time points of myeloid progenitor harvests in days (D) after differentiation initiation. The 2 outlier samples here are the same as those in the hierarchical clustering dendrogram (Figure S3B). PC, principal component.

(C) Transcriptome profile waterfall plots and heatmaps of MIGs of various *FUS* genotypes compared to those of purified human cortical microglia and brain cortex from Galatro et al. (2017). From top to bottom, microglia-enriched genes relative to brain cortex are arranged in decreasing order of expression level, followed by non-enriched genes in increasing order. See Table S4 for lists of microglia-enriched genes in primary human microglia and MIGs.

(D) Spearman's rank correlation coefficients calculated to compare the gene expression profiles of MIGs with, respectively, human primary microglia and brain cortex from Galatro et al. (2017).

(E) Box plots of gene expression level of microglial markers in MIGs across genotypes and time points at which myeloid progenitors were harvested for terminal differentiation. TPM, transcript per million. Presented here are clones from the AG line.



(legend on next page)



engulf dead cells in a relatively immunologically silent manner under homeostatic conditions, a process called efferocytosis (Green et al., 2016). Microglia, as the resident macrophage of the CNS, are tasked to phagocytose apoptotic cells and cellular debris such as myelin fragments. Microglial phagocytosis of dying neurons or degrading myelin has been linked to pathological conditions such as Alzheimer's disease, frontotemporal dementia, and multiple sclerosis (Prinz et al., 2019). With these contexts in mind, we established a live-cell imaging method that quantifies the uptake of apoptotic, commercially available, WT human iPSC-derived motor neurons to assay efferocytosis activity in our MIGs. While the MIGs of the *FUS* genotypic series were capable of phagocytosing apoptotic motor neurons, no dramatic differences were observed in efferocytosis activity in P525L Hom and Het compared to controls. Although a slight upregulated trend was noticeable in Hom compared to other genotypes, the variability across genotypes precluded any statistical significance (Figure 6A). Similarly, we established a myelin phagocytosis assay showing that our MIGs could phagocytose murine myelin fragments, although, again, the differences in activity across genotypes were not statistically significant (Figure S6A).

At the end of the 3-day phagocytosis assays, we collected the cell culture supernatants and profiled cytokines released by MIGs using the Luminex multiplex immunoassay platform. From a panel of 45 cytokines, only 8 were consistently detectable in MIGs, either when untreated or treated with apoptotic motor neurons or myelin. The levels of these detectable cytokines were not dramatically different across treatment conditions or genotypes. Although there may seem to be a trend for increased MIP-1 $\alpha$  in *FUS* P525L Hom compared to controls (Figure S6B),

this was not consistently reproducible in subsequent repeat experiments (data not shown). As a positive control, *Escherichia coli* was applied to the cells, which greatly increased the level of numerous cytokines (Figure S6C), reflecting very similar responses to bacterial lipopolysaccharide in other reported iPSC-derived microglia (Abud et al., 2017) or primary microglia (Rustenhoven et al., 2016). These results confirmed again that our differentiated cells do behave like microglia in their response to pathogens, matching their microglial molecular identity (Prinz et al., 2019).

Koizumi et al. (2007) have demonstrated that when cultured primary rat microglia were treated with exogenous UDP, their phagocytic activity was upregulated as mediated via the chemoreceptor P2RY6, while no chemotactic response was detected. Furthermore, when neuronal cell death was induced in the hippocampal regions of an *in vivo* rat model, the mRNA level of *P2RY6* was increased and the transcripts colocalized with adjacent activated microglia. Based on these findings and considering the upregulation of *P2RY6* in our *FUS* P525L Hom MIGs, UDP was applied to test its effect in our efferocytosis assay. Within the first 24 h of ligand application, an increase in phagocytic activity was seen in MIGs when compared to untreated controls across all genotypes, corroborating what was published by Koizumi and colleagues. However, no differential efferocytosis activities were evident in either P525L Het or Hom cells compared to controls (Figure 6B). In terms of cytokine profiling, UDP-mediated P2RY6 signaling has been shown to increase the level of cytokines such as IL-6, IL-8, macrophage inflammatory protein-1 $\alpha$  (MIP-1 $\alpha$ ), and tumor necrosis factor- $\alpha$  (TNF- $\alpha$ ) in a few myeloid cell culture models (Cox et al., 2005; Garcia et al., 2014; Kim et al., 2011). Although this effect of UDP was largely replicated in our

#### Figure 4. Homozygous *FUS* P525L MIGs display transcriptional perturbations of genes associated with characteristic microglial functions

- (A) Experimental design for large-scale differentiation, RNA-seq, and cryopreservation of MIGs from independent AG and JK lines with various *FUS* control and P525L mutant genotypes. Each box represents a differentiation replicate.
- (B) PCA of RNA-seq transcriptome profiles of MIGs differentiated from AG and JK lines with various *FUS* genotypes as represented by a color code. Two of the outlier samples here are the same as those in the hierarchical clustering dendrogram (Figure S4C); the third had been flagged as an outlier before RNA-seq due to its abnormal fibroblast-like morphology.
- (C) Box plots of differential expression of the *FUS* gene in MIGs with different *FUS* genotypes as determined by RNA-seq.
- (D) Heatmap of differentially expressed genes in *FUS* P525L Hom MIGs as compared independently to WT and Ctrl in both AG and JK lines. Each colored box at the very top represents a differentiation replicate. Displayed names in blue are those of genes associated with GO and MSigDB Canonical Pathways terms linked to microglial features and functions; in bold are GPCR genes selected for further functional studies and *FUS*. See Table S1 for a complete list of and more information on Hom signature genes.
- (E) Top 20 GO terms associated with genes enriched in the P525L Hom signature. In blue are terms linked to characteristic features and functions of microglia. Red bars indicate that the majority of Hom signature genes associated with a term are upregulated. Multiple testing correction was performed using the Benjamini-Hochberg procedure to obtain adjusted p values. See Figure S4A and Table S2 for more gene enrichment analysis results.
- (F) Validation via qRT-PCR of differentially expressed GPCR genes in the Hom signature. See Table S3 for more qRT-PCR validation results of Hom signature genes. Error bars represent standard deviations across the first 3 time points; n = 3.
- \*p < 0.05; \*\*p < 0.01; \*\*\*p < 0.001.

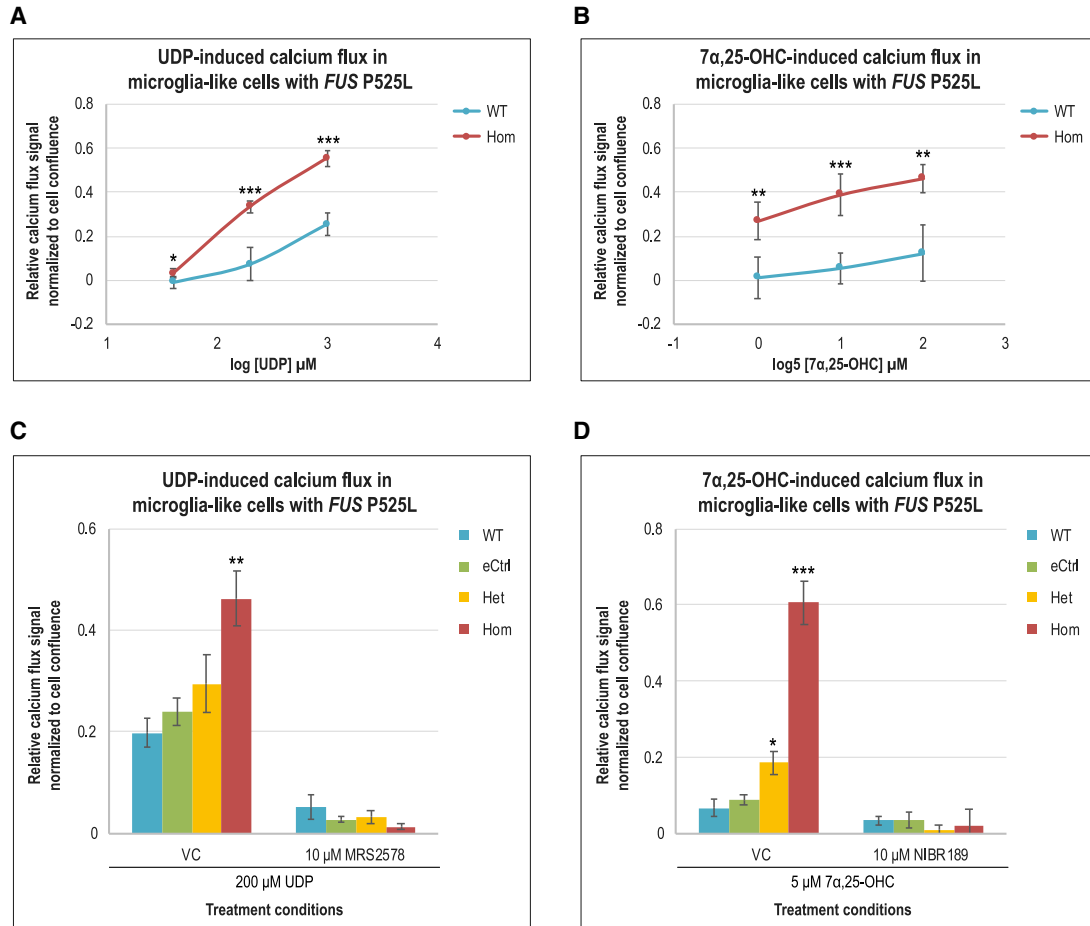


**Figure 5. Differentially expressed chemoreceptor genes in MIGs with *FUS* P525L mutations lead to perturbations of ligand-induced intracellular calcium signaling**

(A and B) Intracellular calcium response to increasing concentrations of (A) UDP or (B)  $7\alpha,25$ -OHC in WT and *FUS* P525L Hom MIGs. (C and D) Intracellular calcium flux in response to (C) UDP or (D)  $7\alpha,25$ -OHC in MIGs of various genotypes. Respectively for the chemoreceptors P2RY6 and GPR183, MRS2578 and NIBR189 are potent specific inhibitors, while ddH<sub>2</sub>O and DMSO serve as vehicle controls (VCs). Error bars represent standard errors of the mean across 3 independent experiments using both AG and JK lines; n = 3. \*p < 0.05; \*\*p < 0.01; \*\*\*p < 0.001.

MIGs, no statistically significant differences were observed in cytokine release across the *FUS* genotypic series under UDP-treated conditions (Figure 6C). Lastly, we noted that despite being a signature gene of P525L Het and Hom MIGs, IL-18 could not be detected in all tested conditions (data not shown).

## DISCUSSION

An increasing number of studies have highlighted the importance of the role that microglia play in neurodegenerative diseases such as ALS (Hickman et al., 2018). However, most of the research to understand microglial involvement uses mouse models overexpressing ALS-linked

mutant proteins. In the case of *FUS*, mice overexpressing WT *FUS* (Mitchell et al., 2013) or an NLS-truncated version of the protein (Funikov et al., 2018) have demonstrated an activated microglia phenotype. Conditioned culture media from astrocytes overexpressing WT *FUS* were also shown to exacerbate pro-inflammatory cytokine production in primary cultures of rat microglia (Ajmone-Cat et al., 2019). Within the human context, the *FUS* P525L mutation has been studied in human iPSC-derived motor neurons where phenotypes such as *FUS* cytoplasmic mislocalization, *FUS* aggregation upon cellular stress, neuronal hypoexcitability, decreased synaptic activity, axonal transport defects, and disruption in DNA damage response signaling have been variously described (Guo et al., 2017; Lenzi et al., 2015; Wang et al., 2019). Despite these findings, questions

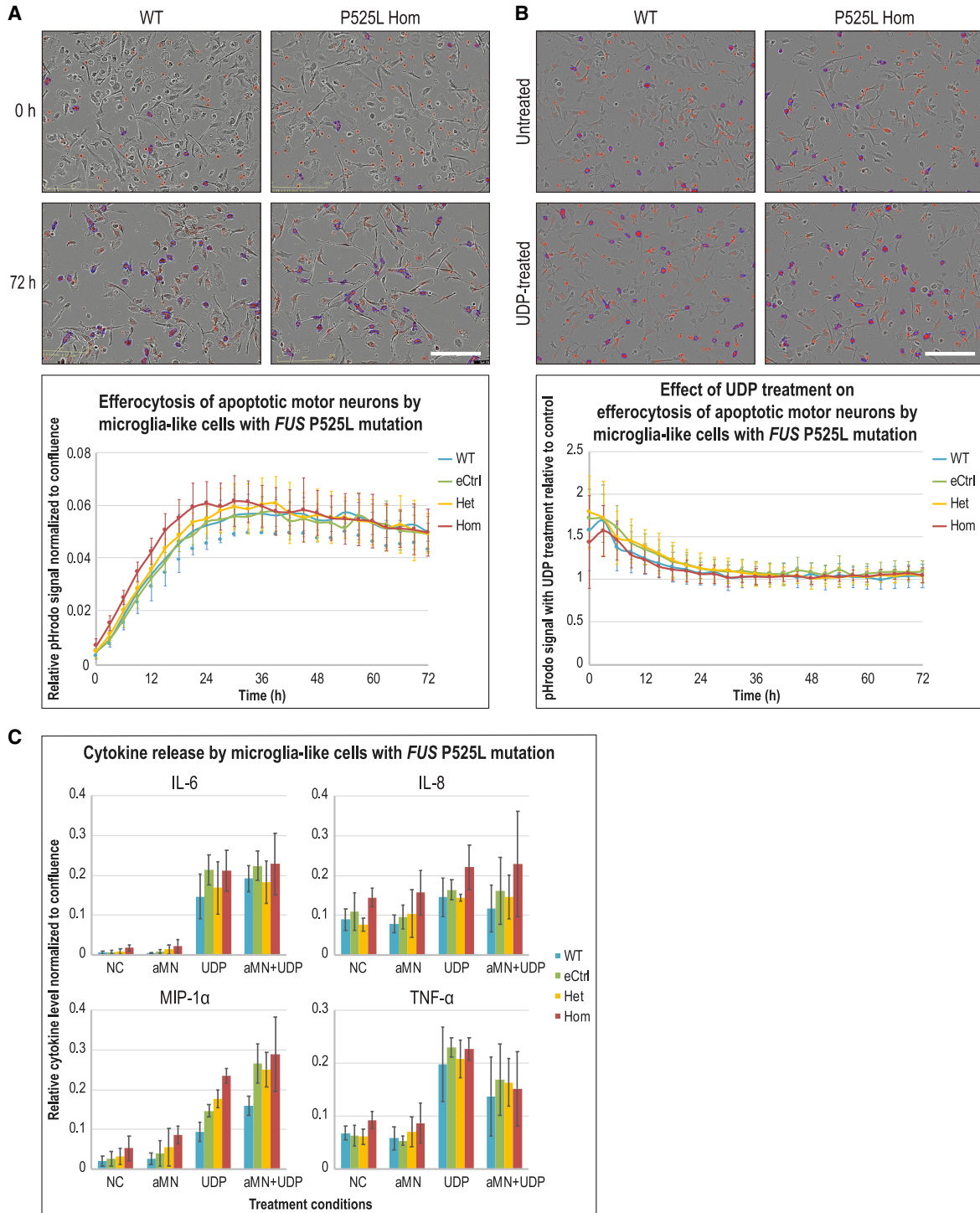


**Figure 6. MIGs with *FUS* P525L mutations do not exhibit phagocytosis or cytokine release phenotypes**

(A and B) Top half of each panel: Phase contrast and pHrodo red fluorescence overlay images of MIGs. pHrodo is a pH-sensitive dye that is almost non-fluorescent at neutral pH but fluoresces brightly (red for our assays) in acidic environments such as phagosomes. However, non-phagocytosed pHrodo-conjugated apoptotic motor neurons had high background fluorescence. To distinguish and exclude this background, efferocytosis activity was defined as pHrodo signals above a threshold area (represented by blue outline masks) because phagocytosed apoptotic motor neurons clustered together in phagosomes of MIGs. Due to space constraints, only representative images of

(legend continued on next page)



of whether and how ALS-linked *FUS* mutations at physiological levels affect human microglia in a cell-autonomous fashion remained unresolved. Our study bridges this knowledge gap.

We first established that human iPSCs carrying *FUS* P525L or complete KO mutations can be successfully differentiated into MIGs where *FUS* protein is mislocalized due to the P525L mutation. Proper microglial differentiation in the context of these mutations was not a given considering that *FUS* KO (Hicks et al., 2000) and homozygous P517L (the murine analog of P525L) knockin (Lyashchenko, 2015) mice die perinatally. We also report that while MIGs respond robustly to *E. coli* in regard to cytokine release, their response to apoptotic motor neurons or murine myelin fragments are seemingly rather muted. We surmise that this could reflect efferocytosis, the homeostatic function of phagocytes such as microglia in clearing up dead cells and debris in an immunologically silent manner (Green et al., 2016). As a technical note, we provide empirical evidence that MIGs differentiated from myeloid progenitors harvested between 50 and 75 days after differentiation initiation are highly comparable in terms of transcriptome profiles.

Our RNA-seq results clearly reveal that homozygous *FUS* P525L mutations perturb the transcriptome profile of MIGs. The P525L Hom signature is enriched for genes associated with several functional properties of microglia. In contrast to Hom, P525L Het MIGs do not exhibit significant transcriptional perturbations. Similarly, the downregulation of specific circular RNAs in iPSC-derived motor neurons observed by Errichelli et al. (2017) occurred in *FUS* P525L homozygotes but not in heterozygotes. This may not be entirely surprising because ALS symptoms caused by heterozygous *FUS* P525L mutation only arise after approximately a decade from birth, and these patients are not known to have congenital developmental defects (Kuang et al., 2017; Shang and Huang, 2016).

Guided by gene enrichment analyses, we focused on the *FUS* P525L Hom signature genes *P2RY6* and *GPR183* to probe whether their transcriptional upregulation translates into a functional alteration in MIGs. We confirmed that ligand activation of these 2 chemoreceptors does induce higher intracellular calcium flux signals in P525L Hom MIGs compared to controls. *P2RY6* is activated by UDP released from damaged or dying cells (Anwar et al., 2020),

and *GPR183* is activated by  $7\alpha,25$ -OHC, a by-product of cholesterol catabolism (Kurschus and Wanke, 2018). These 2 chemoreceptors could be relevant to ALS since neuronal cell death and the breakdown of myelin, which is cholesterol rich, are characteristics of neurodegeneration. In fact, the pro-inflammatory activation of P2 receptors involving *P2RY6* upregulation in the ALS model of SOD1 G93A mutant murine microglia has been reported (D'Ambrasi et al., 2009). Inferring from research performed in other neurodegenerative diseases, we speculate that increased microglial *P2RY6* and *GPR183* signaling could initially play a protective role in ALS by promoting the phagocytosis of dying motor neurons and remyelination, but their prolonged activation would eventually lead to unresolved neuroinflammation and indiscriminate efferocytosis that exacerbates disease at later stages (Anwar et al., 2020; Klejbor et al., 2021).

In addition to *P2RY6*, a few other *FUS* P525L Hom signature genes in our MIGs have been implicated in ALS: *IL18*, *PTGS2*, *TGFB2*, and *TLR7*. The dysregulation of these genes occurs in ALS patients or SOD1 mutant mouse models of the disease and is mostly within the context of neuroinflammation (Berjaoui et al., 2015; Consilvio et al., 2004; Johann et al., 2015; Katsuno et al., 2011). Likewise, the *FUS* overexpression experiments in mouse or cell co-culture models mentioned previously also feature inflammatory activated microglia (Ajmone-Cat et al., 2019; Funikov et al., 2018; Mitchell et al., 2013). Many of these inflammation events have been shown or are likely to be due to microglial responses to neuronal death or other non-cell-autonomous interactions within complex environments. As contrasted in our simpler model, P525L Hom MIGs do not exhibit an overt activated phenotype in terms of increased phagocytosis or inflammatory cytokine release. Therefore, it would be interesting to investigate whether and how *FUS* P525L MIGs interact with other disease-relevant cell types via co-culture or *in vivo* transplantation experiments, which could uncover the relevance of our reported phenotypes to ALS pathogenesis.

Nonetheless, our discovery that homozygous *FUS* P525L mutations cell-autonomously perturb transcriptome profile and chemoreceptor signaling in a human microglia model has shed light on a previously unanswered question. Further research will be required to elucidate the specific mechanism by which homozygous P525L mutations cause

---

WT and *FUS* P525L Hom cells are displayed. Scale bar, 200  $\mu$ m. Bottom half of each panel: (A) Graph for efferocytosis signal normalized to cell confluence versus time from live imaging of MIGs with different *FUS* genotypes. (B) Graph for efferocytosis signal in MIGs of various genotypes treated with UDP relative to signal in untreated control cells versus time. Error bars represent standard deviations across both AG and JK lines, each with 4 replicate wells;  $n = 8$ .

(C) Cytokine release of IL-6, IL-8, MIP-1 $\alpha$  and TNF- $\alpha$  in cell culture supernatant by MIGs under different treatment conditions after 72 h. NC, untreated negative control; aMN, apoptotic motor neurons; UDP, 200  $\mu$ M. Error bars represent standard deviations across both AG and JK lines, each with at least 2 replicate wells;  $n \geq 4$ .



the phenotypes we have observed in human iPSC-derived microglia. The ability to reproducibly scale up microglial differentiation renders future biochemical studies possible to divulge any molecular interactions that could inform how pathological forms of FUS lead to altered microglial function.

## EXPERIMENTAL PROCEDURES

See further details in the [supplemental experimental procedures](#).

### Differential gene expression analysis

Gene expressions were quantified from raw sequencing reads using the OmicSoft ArrayStudio RNA-seq analysis pipeline. Reads that uniquely mapped to the exons of a gene were identified and counted. The resulting read counts were summarized at the gene level as raw expression. Genes were flagged as “absent” or “present” in each sample using an empirical minimum raw read count of 10. For comparisons between 2 groups of samples, genes that were not flagged as present in all of the samples of the higher-expressing group were excluded. Differential gene expression levels were then analyzed using the DESeq2 method (Love et al., 2014). Briefly, raw read counts across samples were normalized to adjust for variation in sequencing depth. Dispersion of expression was estimated by sharing information across genes with similar expression levels and a negative binomial generalized linear model was constructed. Fold-change was computed as the effect size of the treatment, which reflects the difference in expression levels between 2 groups. The statistical significance of differential expression levels was assessed by the Wald test. Lastly, we defined genes with fold-changes of no less than 1.5 in either up or down direction with  $p < 0.01$  as significantly perturbed gene signatures.

### Intracellular calcium flux assay

MIGs were plated at  $1 \times 10^4$  cells per well into flat clear-bottom black-walled poly-D-lysine-coated 96-well plates (Greiner, cat. no. 655946). At least 2 days later, an intracellular calcium flux assay was performed using the FLIPR Calcium 6 Assay Kit (Molecular Devices, cat. no. R8190) according to the manufacturer's protocol. Briefly, plated cells were incubated with calcium indicator dye containing 2.5 mM probenecid (Invitrogen, cat. no. P36400) for 2 h at 37 °C. When chemoreceptor inhibitors were used, they were applied at this step. Chemoreceptor ligands were prepared at the desired concentrations and aliquoted into V-bottom 96-deep well plates (Axygen, cat. no. P-96-450V-C-S). Assays were performed by measuring calcium indicator fluorescence intensity immediately upon ligand addition every second for 400 s on the FLIPR Tetra High-throughput Cellular Screening System with ICCD camera using ScreenWorks software (Molecular Devices). See the [supplemental experimental procedures](#) for more detailed information.

### Data and code availability

The accession number for the RNA-seq datasets generated in this paper is GEO: GSE172459. The datasets from Galatro et al. are available through GEO: GSE99074.

## SUPPLEMENTAL INFORMATION

Supplemental information can be found online at <https://doi.org/10.1016/j.stemcr.2022.01.004>.

## AUTHOR CONTRIBUTIONS

Conceptualization, S.Y.K. and E.C.; methodology, S.Y.K., E.C., C.H., and J.K.; software, Y.B.; investigation, S.Y.K., J.S., P.L., J.N., K.L., N.C., A.C., Q.T., J.E., H.J., and C.F.; data curation, S.Y.K. and Y.B.; formal analysis, S.Y.K., Y.B., and T.Y.; validation, S.Y.K.; visualization, S.Y.K. and Y.B.; writing – original draft, S.Y.K.; writing – review & editing, S.Y.K., E.C., and B.Z.; supervision, E.C., B.Z., S.Y.K., and Y.B.

## CONFLICTS OF INTERESTS

All of the authors are current or former employees of Regeneron Pharmaceuticals.

## ACKNOWLEDGMENTS

We thank Meghan Drummond for providing expertise in CRISPR reagent design, Daria Zamolodchikov for providing the pHrodo-conjugated murine myelin fragment reagent, and many of our colleagues in Velocigen and across Regeneron for making this project possible. We also thank Drummond and Zamolodchikov again, as well as Kevin Kanning and Aarti Sharma for providing insightful comments on the manuscript.

Received: April 28, 2021

Revised: January 5, 2022

Accepted: January 6, 2022

Published: March 8, 2022

## REFERENCES

- Abud, E.M., Ramirez, R.N., Martinez, E.S., Healy, L.M., Nguyen, C.H.H., Newman, S.A., Yeromin, A.V., Scarfone, V.M., Marsh, S.E., Fimbres, C., et al. (2017). iPSC-derived human microglia-like cells to study neurological diseases. *Neuron* 94, 278–293.e9.
- Ajmone-Cat, M.A., Onori, A., Toselli, C., Stronati, E., Morlando, M., Bozzoni, I., Monni, E., Kokaia, Z., Lupo, G., Minghetti, L., et al. (2019). Increased FUS levels in astrocytes leads to astrocyte and microglia activation and neuronal death. *Sci. Rep.* 9, 4572.
- Anwar, S., Pons, V., and Rivest, S. (2020). Microglia purinoceptor P2Y6: an emerging therapeutic target in CNS diseases. *Cells* 9, 1595.
- Bennett, M.L., Bennett, F.C., Liddelov, S.A., Ajami, B., Zamanian, J.L., Fernhoff, N.B., Mulinyawe, S.B., Bohlen, C.J., Adil, A., Tucker, A., et al. (2016). New tools for studying microglia in the mouse and human CNS. *Proc. Natl. Acad. Sci. U S A* 113, E1738–E1746.
- Berjaoui, S., Povedano, M., Garcia-Esparcia, P., Carmona, M., Aso, E., and Ferrer, I. (2015). Complex inflammation mRNA-related response in ALS is region dependent. *Neural Plast.* 2015, 573784.
- Butovsky, O., Jedrychowski, M.P., Moore, C.S., Cialic, R., Lanser, A.J., Gabriely, G., Koeglsperger, T., Dake, B., Wu, P.M., Doykan, C.E., et al. (2014). Identification of a unique TGF-beta-dependent



- molecular and functional signature in microglia. *Nat. Neurosci.* *17*, 131–143.
- Clarke, B.E., and Patani, R. (2020). The microglial component of amyotrophic lateral sclerosis. *Brain* *143*, 3526–3539.
- Consilvio, C., Vincent, A.M., and Feldman, E.L. (2004). Neuroinflammation, COX-2, and ALS—a dual role? *Exp. Neurol.* *187*, 1–10.
- Cox, M.A., Gomes, B., Palmer, K., Du, K., Wiekowski, M., Wilburn, B., Petro, M., Chou, C.C., Desquitado, C., Schwarz, M., et al. (2005). The pyrimidinergic P2Y<sub>6</sub> receptor mediates a novel release of proinflammatory cytokines and chemokines in monocytic cells stimulated with UDP. *Biochem. Biophys. Res. Commun.* *330*, 467–473.
- D'Ambrosi, N., Finocchi, P., Apolloni, S., Cozzolino, M., Ferri, A., Padovano, V., Pietrini, G., Carri, M.T., and Volonte, C. (2009). The proinflammatory action of microglial P2 receptors is enhanced in SOD1 models for amyotrophic lateral sclerosis. *J. Immunol.* *183*, 4648–4656.
- Douvaras, P., Sun, B., Wang, M., Kruglikov, I., Lallo, G., Zimmer, M., Terrenoire, C., Zhang, B., Gandy, S., Schadt, E., et al. (2017). Directed differentiation of human pluripotent stem cells to microglia. *Stem Cell Rep.* *8*, 1516–1524.
- Erichelli, L., Dini Modigliani, S., Laneve, P., Colantoni, A., Legnini, I., Caputo, D., Rosa, A., De Santis, R., Scarfo, R., Peruzzi, G., et al. (2017). FUS affects circular RNA expression in murine embryonic stem cell-derived motor neurons. *Nat Commun* *8*, 14741.
- Funikov, S.Y., Rezvykh, A.P., Mazin, P.V., Morozov, A.V., Maltsev, A.V., Chicheva, M.M., Vikhareva, E.A., Evgen'ev, M.B., and Ustyugov, A.A. (2018). FUS(1-359) transgenic mice as a model of ALS: pathophysiological and molecular aspects of the proteinopathy. *Neurogenetics* *19*, 189–204.
- Galatro, T.F., Holtman, I.R., Lerario, A.M., Vainchtein, I.D., Brouwer, N., Sola, P.R., Veras, M.M., Pereira, T.F., Leite, R.E.P., Moller, T., et al. (2017). Transcriptomic analysis of purified human cortical microglia reveals age-associated changes. *Nat. Neurosci.* *20*, 1162–1171.
- Garcia, R.A., Yan, M., Search, D., Zhang, R., Carson, N.L., Ryan, C.S., Smith-Monroy, C., Zheng, J., Chen, J., Kong, Y., et al. (2014). P2Y<sub>6</sub> receptor potentiates pro-inflammatory responses in macrophages and exhibits differential roles in atherosclerotic lesion development. *PLoS One* *9*, e111385.
- Ginhoux, F., Lim, S., Hoeffel, G., Low, D., and Huber, T. (2013). Origin and differentiation of microglia. *Front Cell Neurosci* *7*, 45.
- Gosselin, D., Skola, D., Coufal, N.G., Holtman, I.R., Schlachetzki, J.C.M., Sajti, E., Jaeger, B.N., O'Connor, C., Fitzpatrick, C., Pasillas, M.P., et al. (2017). An environment-dependent transcriptional network specifies human microglia identity. *Science* *356*, eaal3222.
- Green, D.R., Oguin, T.H., and Martinez, J. (2016). The clearance of dying cells: table for two. *Cell Death Differ* *23*, 915–926.
- Guo, W., Naujock, M., Fumagalli, L., Vandoorne, T., Baatsen, P., Boon, R., Ordovas, L., Patel, A., Welters, M., Vanwelden, T., et al. (2017). HDAC6 inhibition reverses axonal transport defects in motor neurons derived from FUS-ALS patients. *Nat. Commun.* *8*, 861.
- Hickman, S., Izzy, S., Sen, P., Morsett, L., and El Khoury, J. (2018). Microglia in neurodegeneration. *Nat. Neurosci.* *21*, 1359–1369.
- Hickman, S.E., Kingery, N.D., Ohsumi, T.K., Borowsky, M.L., Wang, L.C., Means, T.K., and El Khoury, J. (2013). The microglial sensome revealed by direct RNA sequencing. *Nat. Neurosci.* *16*, 1896–1905.
- Hicks, G.G., Singh, N., Nashabi, A., Mai, S., Bozek, G., Klewes, L., Arapovic, D., White, E.K., Koury, M.J., Oltz, E.M., et al. (2000). Fus deficiency in mice results in defective B-lymphocyte development and activation, high levels of chromosomal instability and perinatal death. *Nat. Genet.* *24*, 175–179.
- Ji, A.L., Zhang, X., Chen, W.W., and Huang, W.J. (2017). Genetics insight into the amyotrophic lateral sclerosis/frontotemporal dementia spectrum. *J. Med. Genet.* *54*, 145–154.
- Johann, S., Heitzer, M., Kanagaratnam, M., Goswami, A., Rizo, T., Weis, J., Troost, D., and Beyer, C. (2015). NLRP3 inflammasome is expressed by astrocytes in the SOD1 mouse model of ALS and in human sporadic ALS patients. *Glia* *63*, 2260–2273.
- Katsuno, M., Adachi, H., Banno, H., Suzuki, K., Tanaka, F., and Sobue, G. (2011). Transforming growth factor-beta signaling in motor neuron diseases. *Curr. Mol. Med.* *11*, 48–56.
- Kim, B., Jeong, H.K., Kim, J.H., Lee, S.Y., Jou, I., and Joe, E.H. (2011). Uridine 5'-diphosphate induces chemokine expression in microglia and astrocytes through activation of the P2Y<sub>6</sub> receptor. *J. Immunol.* *186*, 3701–3709.
- Klejbtor, I., Shimshek, D.R., Klimaszczyńska-Lata, J., Velasco-Estevez, M., Morys, J., Karaszewski, B., Szutowicz, A., and Rutkowska, A. (2021). EBI2 is expressed in glial cells in multiple sclerosis lesions, and its knock-out modulates remyelination in the cuprizone model. *Eur. J. Neurosci.* *54*, 5173–5188.
- Koizumi, S., Shigemoto-Mogami, Y., Nasu-Tada, K., Shinozaki, Y., Ohsawa, K., Tsuda, M., Joshi, B.V., Jacobson, K.A., Kohsaka, S., and Inoue, K. (2007). UDP acting at P2Y<sub>6</sub> receptors is a mediator of microglial phagocytosis. *Nature* *446*, 1091–1095.
- Kuang, L., Kamelgarn, M., Arenas, A., Gal, J., Taylor, D., Gong, W., Brown, M., St Clair, D., Kasarskis, E.J., and Zhu, H. (2017). Clinical and experimental studies of a novel P525R FUS mutation in amyotrophic lateral sclerosis. *Neurol. Genet.* *3*, e172.
- Kurschus, F.C., and Wanke, F. (2018). EBI2 - sensor for dihydroxycholesterol gradients in neuroinflammation. *Biochimie* *153*, 52–55.
- Lavin, Y., Winter, D., Blecher-Gonen, R., David, E., Keren-Shaul, H., Merad, M., Jung, S., and Amit, I. (2014). Tissue-resident macrophage enhancer landscapes are shaped by the local microenvironment. *Cell* *159*, 1312–1326.
- Lee, M.H., Appleton, K.M., El-Shewy, H.M., Sorci-Thomas, M.G., Thomas, M.J., Lopes-Virella, M.F., Luttrell, L.M., Hammad, S.M., and Klein, R.L. (2017). S1P in HDL promotes interaction between SR-BI and S1PR1 and activates S1PR1-mediated biological functions: calcium flux and S1PR1 internalization. *J. Lipid Res.* *58*, 325–338.
- Lenzi, J., De Santis, R., de Turreis, V., Morlando, M., Laneve, P., Calvo, A., Caliendo, V., Chio, A., Rosa, A., and Bozzoni, I. (2015). ALS mutant FUS proteins are recruited into stress granules in induced pluripotent stem cell-derived motoneurons. *Dis. Model Mech.* *8*, 755–766.
- Li, Q., and Barres, B.A. (2018). Microglia and macrophages in brain homeostasis and disease. *Nat. Rev. Immunol.* *18*, 225–242.



- Liao, F., Shirakawa, A.K., Foley, J.F., Rabin, R.L., and Farber, J.M. (2002). Human B cells become highly responsive to macrophage-inflammatory protein-3 alpha/CC chemokine ligand-20 after cellular activation without changes in CCR6 expression or ligand binding. *J. Immunol.* *168*, 4871–4880.
- Lo Bello, M., Di Fini, F., Notaro, A., Spataro, R., Conforti, F.L., and La Bella, V. (2017). ALS-related mutant FUS protein is mislocalized to cytoplasm and is recruited into stress granules of fibroblasts from asymptomatic FUS P525L mutation carriers. *Neurodegener Dis.* *17*, 292–303.
- Love, M.I., Huber, W., and Anders, S. (2014). Moderated estimation of fold change and dispersion for RNA-seq data with DESeq2. *Genome Biol.* *15*, 550.
- Lyashchenko, A.K. (2015). Mechanisms of FUS-Mediated Motor Neuron Degeneration in Amyotrophic Lateral Sclerosis (Columbia University).
- Mitchell, J.C., McGoldrick, P., Vance, C., Hortobagyi, T., Sreedharan, J., Rogelj, B., Tudor, E.L., Smith, B.N., Klasen, C., Miller, C.C., et al. (2013). Overexpression of human wild-type FUS causes progressive motor neuron degeneration in an age- and dose-dependent fashion. *Acta Neuropathol.* *125*, 273–288.
- Muffat, J., Li, Y., Yuan, B., Mitalipova, M., Omer, A., Corcoran, S., Bakiasi, G., Tsai, L.H., Aubourg, P., Ransohoff, R.M., et al. (2016). Efficient derivation of microglia-like cells from human pluripotent stem cells. *Nat. Med.* *22*, 1358–1367.
- Naumann, M., Peikert, K., Gunther, R., van der Kooij, A.J., Aronica, E., Hubers, A., Danel, V., Corcia, P., Pan-Montojo, F., Cirak, S., et al. (2019). Phenotypes and malignancy risk of different FUS mutations in genetic amyotrophic lateral sclerosis. *Ann. Clin. Transl. Neurol.* *6*, 2384–2394.
- Pandya, H., Shen, M.J., Ichikawa, D.M., Sedlock, A.B., Choi, Y., Johnson, K.R., Kim, G., Brown, M.A., Elkahloun, A.G., Maric, D., et al. (2017). Differentiation of human and murine induced pluripotent stem cells to microglia-like cells. *Nat. Neurosci.* *20*, 753–759.
- Portz, B., Lee, B.L., and Shorter, J. (2021). FUS and TDP-43 phases in health and disease. *Trends Biochem. Sci.* *46*, 550–563.
- Preuss, I., Ludwig, M.G., Baumgarten, B., Bassilana, F., Gessier, F., Seuwen, K., and Sailer, A.W. (2014). Transcriptional regulation and functional characterization of the oxysterol/EBI2 system in primary human macrophages. *Biochem. Biophys. Res. Commun.* *446*, 663–668.
- Prinz, M., Jung, S., and Priller, J. (2019). Microglia biology: one century of evolving concepts. *Cell* *179*, 292–311.
- Rustenhoven, J., Park, T.I., Schweder, P., Scotter, J., Correia, J., Smith, A.M., Gibbons, H.M., Oldfield, R.L., Bergin, P.S., Mee, E.W., et al. (2016). Isolation of highly enriched primary human microglia for functional studies. *Sci. Rep.* *6*, 19371.
- Shang, Y., and Huang, E.J. (2016). Mechanisms of FUS mutations in familial amyotrophic lateral sclerosis. *Brain Res.* *1647*, 65–78.
- Souza, P.V., Pinto, W.B., Chieia, M.A., and Oliveira, A.S. (2015). Clinical and genetic basis of familial amyotrophic lateral sclerosis. *Arq Neuropsiquiatr* *73*, 1026–1037.
- Taylor, J.P., Brown, R.H., Jr., and Cleveland, D.W. (2016). Decoding ALS: from genes to mechanism. *Nature* *539*, 197–206.
- Tyzack, G.E., Luisier, R., Taha, D.M., Neeves, J., Modic, M., Mitchell, J.S., Meyer, I., Greensmith, L., Newcombe, J., Ule, J., et al. (2019). Widespread FUS mislocalization is a molecular hallmark of amyotrophic lateral sclerosis. *Brain* *142*, 2572–2580.
- Wang, H., Rangaswamy, S., Kodavati, M., Mitra, J., Guo, W., Guerero, E.N., Van Den Bosch, L., and Hegde, M.L. (2019). RT(2) PCR array screening reveals distinct perturbations in DNA damage response signaling in FUS-associated motor neuron disease. *Mol. Brain* *12*, 103.
- Wang, Y., Szretter, K.J., Vermi, W., Gilfillan, S., Rossini, C., Cella, M., Barrow, A.D., Diamond, M.S., and Colonna, M. (2012). IL-34 is a tissue-restricted ligand of CSF1R required for the development of Langerhans cells and microglia. *Nat. Immunol.* *13*, 753–760.
- Weisheit, I., Kroeger, J.A., Malik, R., Klimmt, J., Crusius, D., Danert, A., Dichgans, M., and Paquet, D. (2020). Detection of deleterious on-target effects after HDR-mediated CRISPR editing. *Cell Rep* *31*, 107689.
- Xu, D., Jin, T., Zhu, H., Chen, H., Ofengeim, D., Zou, C., Mifflin, L., Pan, L., Amin, P., Li, W., et al. (2018). TBK1 suppresses RIPK1-driven apoptosis and inflammation during development and in aging. *Cell* *174*, 1477–1491.
- Yang, L., Zhang, J., Kamelgarn, M., Niu, C., Gal, J., Gong, W., and Zhu, H. (2015). Subcellular localization and RNAs determine FUS architecture in different cellular compartments. *Hum. Mol. Genet.* *24*, 5174–5183.
- Zhang, Y., Sloan, S.A., Clarke, L.E., Caneda, C., Plaza, C.A., Blumenthal, P.D., Vogel, H., Steinberg, G.K., Edwards, M.S., Li, G., et al. (2016). Purification and characterization of progenitor and mature human astrocytes reveals transcriptional and functional differences with mouse. *Neuron* *89*, 37–53.
- Zhou, Y., Liu, S., Liu, G., Ozturk, A., and Hicks, G.G. (2013). ALS-associated FUS mutations result in compromised FUS alternative splicing and autoregulation. *PLoS Genet.* *9*, e1003895.